REVISTA MATÉRIA V.27 N.04
ISSN 1517-7076 articles e20220170, 2022

Characterization of induction hardened and tempered AISI 1045 steel

G.D. Wenish[1], M. Prince[2], J. Maniraj[3]

[1]Department of Mechanical Engineering, Ponjesly College of Engineering, Nagercoil, Tamilnadu, India.

[2]Solamalai College of Engineering, Madurai, Tamilnadu, India.

[3]Department of Mechanical Engineering, Kalaignar Karunanidhi Institute of Technology, Kannampalayam, Coimbatore, Tamilnadu, India.

e-mail: wenishgd@gmail.com, Drprince1977@gmail.com, drmani79@gmail.com

ABSTRACT

In this investigation of AISI 1045 steel are tested in two stages. In the first stage of AISI 1045 steel samples, induction boriding and induction hardening of heat treatment typically 800 °C, 900 °C, 1000 °C, 1100 °C, and 1200 °C applied over the course of two seconds. Internal strains maybe mitigated using a 30 min tempering at temperature ranges 300 °C, 500 °Cand 700 °C. After that the samples subjected to the induction hardening, microhardness and tensile strength according to ASTM. The lowest hardness readings are achieved between 800 and 1100 °C, while the maximum hardness of 685HV is reported after heating to 1200 °C and then cooling in water. The second stage involves AISI 1045 steel is treated with low-temperature plasma nitro-carburizing, and its effects are studied. The specimens are treated at temperatures over 430 °C, NCr_2 is formed and has an effect on the corrosion resistance property. Increasing the temperature to 450 °C raises the surface hardness to approximately 1000 $HV_{0.05}$. Treatment at 400 °C results in superior corrosion resistance compared to untreated steel. According to the results of the experiments, the surface hardness of AISI 1045 steel materials increases with an increase in temperature.

Keywords: Induction Hardening; Quenching; Tempering; Microhardness; Austenitic Stainless Steel; Plasma Nitro-Carburizing.

1. INTRODUCTION

Materials engineering advancements have improved materials and shed light on technical, environmental, and societal issues [1, 2]. When making a product, the choice of materials is of paramount importance. In the industrial sector, high-tech iron and steel materials are valued for their extensive mechanical qualities [3, 4]. Sulfur, selenium, copper, lead, aluminium, and calcium are only some of the alloying elements that may be modified in stainless steel during melting in order to tailor the material's machinability [5]. Because of its many high-tech uses, stainless steel is often expected to be tough and scratch-proof [6]. Surface hardness, scratch resistance, and wear resistance may all be increased by the use of procedures that have been proven effective in industry [7].

With induction hardening, a hardened surface layer is formed while the underlying microstructure remains unchanged, improving wear resistance, surface toughness, and fatigue condition [8–11]. The resultant hardened area improves the material's strength in addition to its wear and fatigue resistance. Although through hardening may improve toughness, it may not be as effective in improving resistance to surface indentation, fatigue, and wear as induction hardening [12–15]. The hardness and microstructure could be accurately predicted using the started simulation technique, making it useful for induction hardening process design and improvement [16].

AISI 1045 steel's mechanical and tribological properties are compared with those of unmodified and pulse-magnetized steel [17]. The hard machining tests were conducted to determine the effect that induction heating had on the microstructure and residual stresses of AISI 4340 steel prior to machining. Induction hardening is only capable of strengthening martensitic stainless steel [18]. The carbon content of the steel, the temperature to which the steel is heated prior to quick quenching, and the temperature and duration of quenching during the tempering of the martensite are all crucial factors in the hardening process and the overall work as shown in Figure 1.

Corresponding Author: G.D. Wenish Received on 12/07/2022 Accepted on 20/07/2022

DOI: https://doi.org/10.1590/1517-7076-RMAT-2022-0170

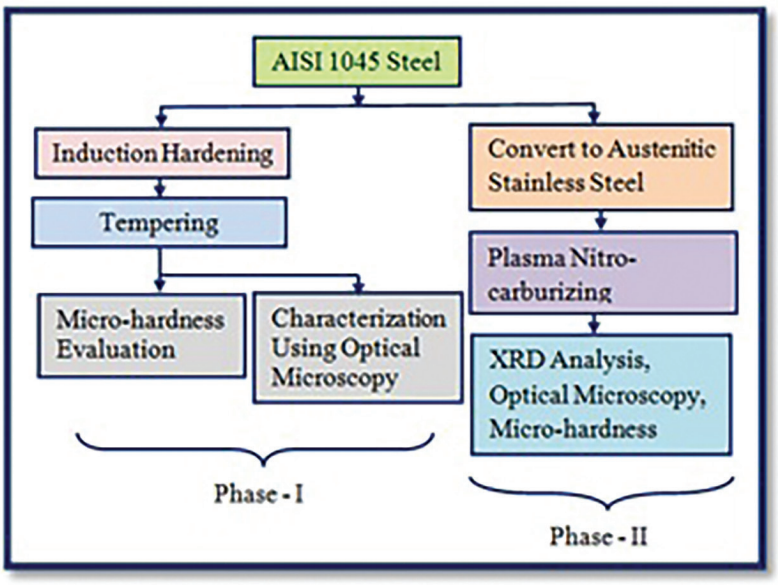

Figure 1: The framework of proposed research work.

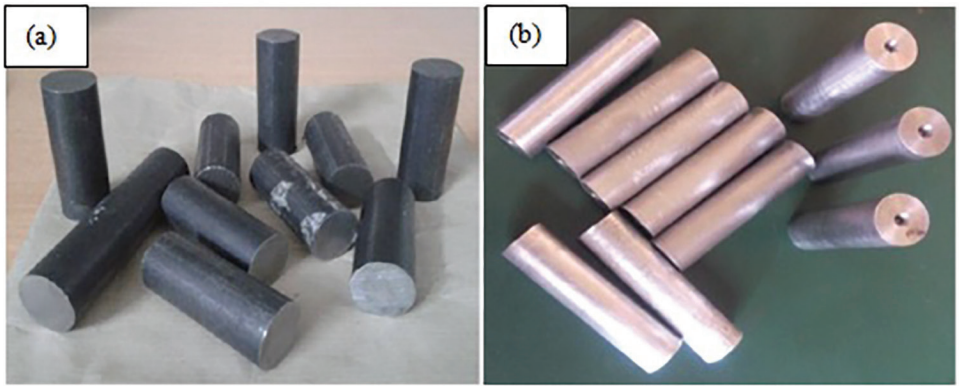

Figure 2: The experimental specimens of (a) AISI 1045 steel and (b) AISI steel after surface finishing.

2. EXPERIMENTAL METHODS AND TESTING

2.1. AISI 1045 steel

The 1045 steel is medium tensile steel that is typically supplied in black hot rolled. The SAE-AISI 1045 rod-shaped steel materials were chosen for the experiments because they have ferrite and pearlite structures and may benefit from induction hardening to increase their surface hardness [19]. The chemical elements in AISI 1045 steel as shown in Table 1 and the mechanical properties indicated in Table 2. The experimental specimen of AISI 1045 steel has 25 mm in diameter and 75 mm in length as indicated in Figure 2 (a). The AISI steel has been polished to a mirror finish, and the specimen has been machined in a lathe to generate a glassy smooth surface (very low depth of cut) that facilitates the entry of carbon atoms during heating from the boriding paste as shown in Figure 2 (b).

2.2. Boride paste

Boriding is a heat and chemical treatment that uniformly coats metals with boron. Certain materials' surfaces and hardness may be improved by applying a boride paste on top of them [20]. This is a breakdown of the components that make up boriding paste and the relative amounts of those components. Silicon carbide components are the most common in boride paste, accounting for half of the total. Sodium carbonate and titanium dioxide are present in the boride paste composites, although only at trace amounts as shown in Table 3.

Table 1: The chemical composition of AISI 1045 steel.

MATERIALS	C	Fe	Si	Mn	P	Cr	W	Al
Weight (%)	0.43	98.41	0.18	0.76	0.012	0.004	0.013	0.04

Table 2: The mechanical properties of AISI 1045 steel.

PROPERTIES	VALUES
Tensile Strength (Mpa)	570–700
Yield Strength (Mpa)	300–450
Elongation in (%)	14–30
Hardness Brinell (HB)	170–210

Table 3: The chemical composition of boriding paste.

NAME OF THE COMPOSITIONS	WEIGHT (%)
Boron Carbide (B_4C)	30
Silicon Carbide (SiC)	50
Potassium Tetra Fluro Borate (KbF_4)	10
Sodium carbonate (Na_2CO_3)	5
Titanium Dioxide (TiO_3)	5

Figure 3: AISI 1045 steel specimen after applying boride paste.

3. CHARACTERIZATION OF AISI 1045 STEEL

3.1. Induction boriding process

Steels coated in a layer of boron oxide have wear resistance on par with sintered carbides. Boriding is proposed for the medium carbon steel AISI 1045, with dimensions chosen per ASTM standards. The dimensions of the sample are 70 mm in length and 20 mm in width. Boroiding produces a surface hardness in the range of 1400–2100 HV. Boride paste was spread evenly on the test specimen with great care. Figure 3 shows the boride paste that was slathered over the surface is still damp. Drying it out in the sun for 30 minutes is required before it can be used for surface hardening. A paste made of borates may be applied to a material's surface to restore its hardness and other qualities.

3.2. Induction surface hardening

The heat treatment process involves a series of temperatures and times of 2 seconds each: Steel was used in the experiments at temperatures of 800 °C, 900 °C, 1000 °C, 1100 °C, and 1200 °C is used with dimensions of 25 mm in diameter and 75 mm in length. ASKS industries in Coimbatore, Tamilnadu perform the induction hardening process on 1045 steel.

Specimens are made out of AISI 1045 steel rod material and put into the induction coil for testing. The transformer is what supplies the energy to heat the coil. The induction coil is linked to the transformer, which receives the AC 240 V, 15 Amps. This mechanism is used for the purpose of tempering AISI 1045 steel. The induction heating process and the line diagram is shown in Figure 4(a) & (b).

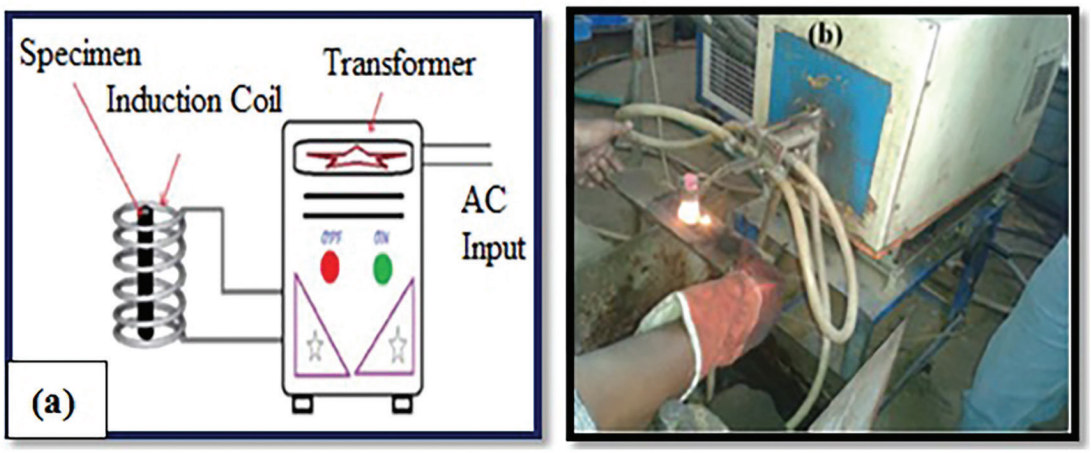

Figure 4: Induction heating apparatus (a) line diagram (b) induction heating process.

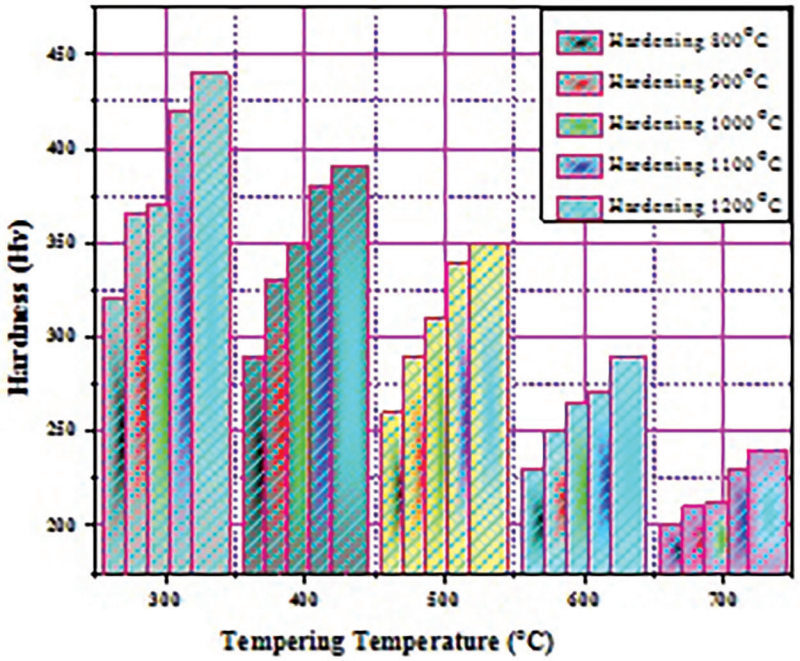

Figure 5: The surface hardness of tempering steel of AISI 1045.

3.3. Surface tempering process

After hardening processes the tempering treatments were applied. The samples are air cooled after being heated to 300 °C, 500 °C, and 700 °C for 30 minutes in a furnace.

3.3.1. Microhardness of hardened 1045 steel

Using a Vickers hardness tester, find the induction hardened AISI 1045 steel have a micro-hardness of 685 HV at a temperature of about 1200 °C. A micro-hardness of 464 HV was recorded at the 800 °C hardening temperature used in the experiments. It is clear that, even at the highest temperature, an entirely austenitic structure is not created. The micro-hardness value of 439 HV at a hardening temperature of 1200 °C is higher than the values of 344 HV at 500 °C and 223 HV at 700 °C, respectively. The hardness of the undisturbed substrate was measured at 130 HV. Increasing the tempering temperature results in a marked reduction in surface hardness, which is a structural signature of the phase transition as shown in Figure 5. The hardened layer is thinner because of the decreased hardening temperature compared to when it was treated at 1200 °C. A thinner hardened layer may be achieved by raising the tempering temperature [21].

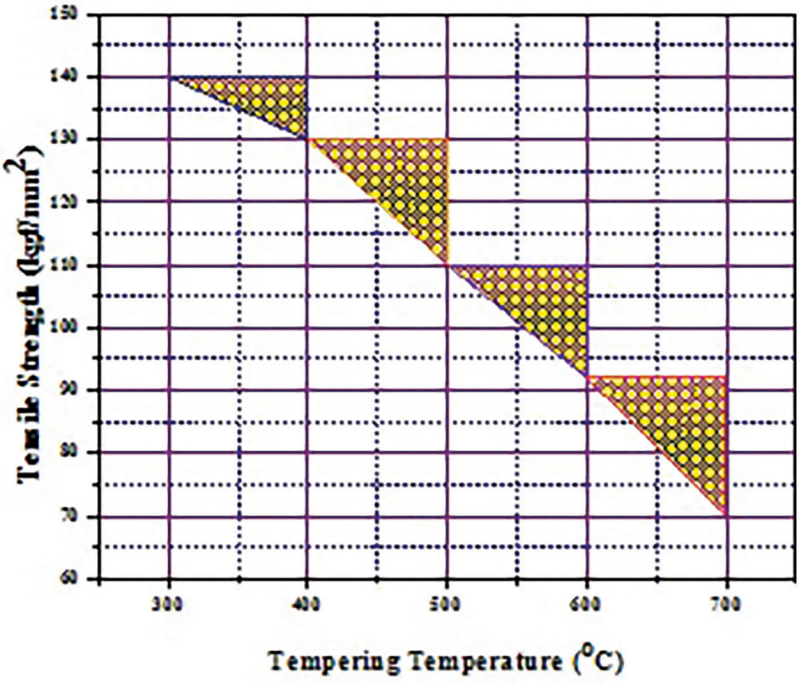

Figure 6: The tensile strength of the tempered steel specimen.

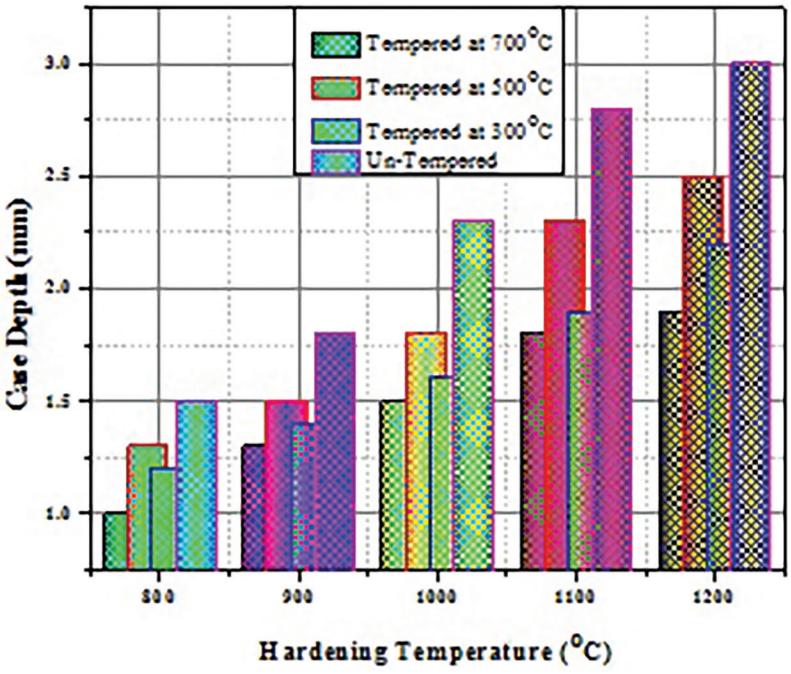

Figure 7: The relationship between case depth and hardening temperature of the specimen.

3.3.2. Tensile strength

Figure 6 shows that the specimen's tensile strength diminishes as the tempering temperature rises. When the specimen was hardened to over 1200 °C and tempered to around 300 °C, the tensile strength was 143.6 kgf /mm^2. Furthermore, after hardening and tempering at 500 °C, the tensile strength dropped in 111.42 kgf/mm^2. A significant decreases in hardness occurred when hardened steel was tempered [22, 23]. However, tempering is necessary for reducing internal stresses and creating a microstructure of ferrite and distributed carbide, both of which significantly enhance toughness. All tests are conducted on materials that have not been tempered or on materials that have been tempered at 300 °C, 500 °C, and 700 °C. The case depth grows as the hardening temperature rises and the inductor speed increases, the case depth values decrease as shown in Figure 7 and 8.

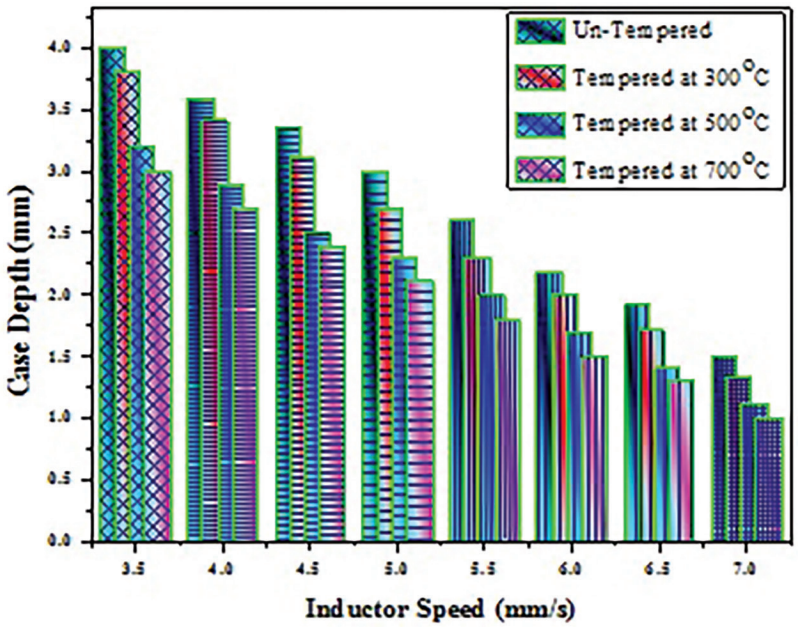

Figure 8: The relationship between case depth and inductor speed of the specimen.

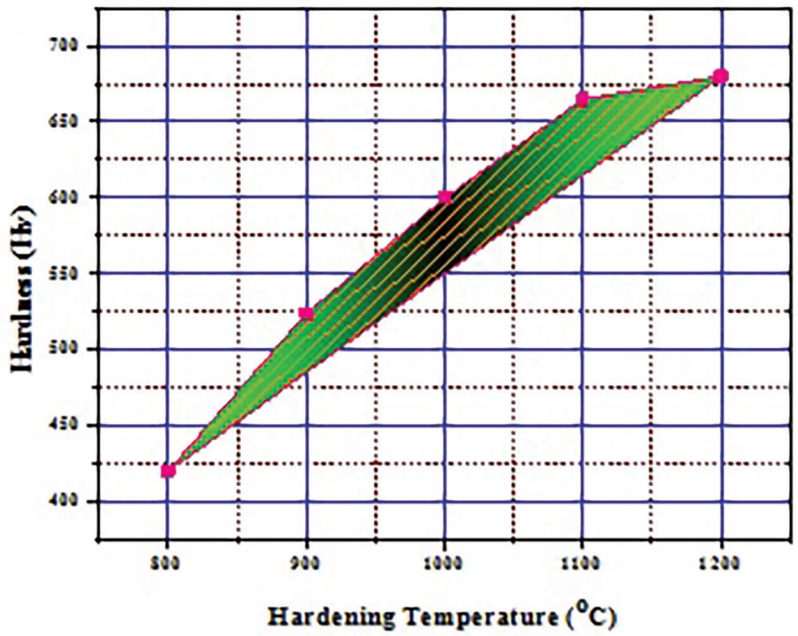

Figure 9: The surface hardness of hardened material of AISI 1045.

3.4. Characterization of processed AISI 1045 steel

3.4.1. Vickers hardness testing

Specimens of induction-hardened 1045 steel had their microhardness tested using Vickers hardness testing equipment with a weight of 5 kg at intervals of 0.50 mm. Before optical microscopy can be used to examine the microstructure, the sample cross-sections must be mechanically polished by double disc polishing machine and etched using acetone solution. Figure 9 displays the relationship between surface hardness and hardening temperature for AISI 1045 steel. These charts illustrate the linear relationship between cumulative hardening temperature and an increase in surface hardness. At a maximum temperature of 1200 °C, the surface hardness reached its maximum value.

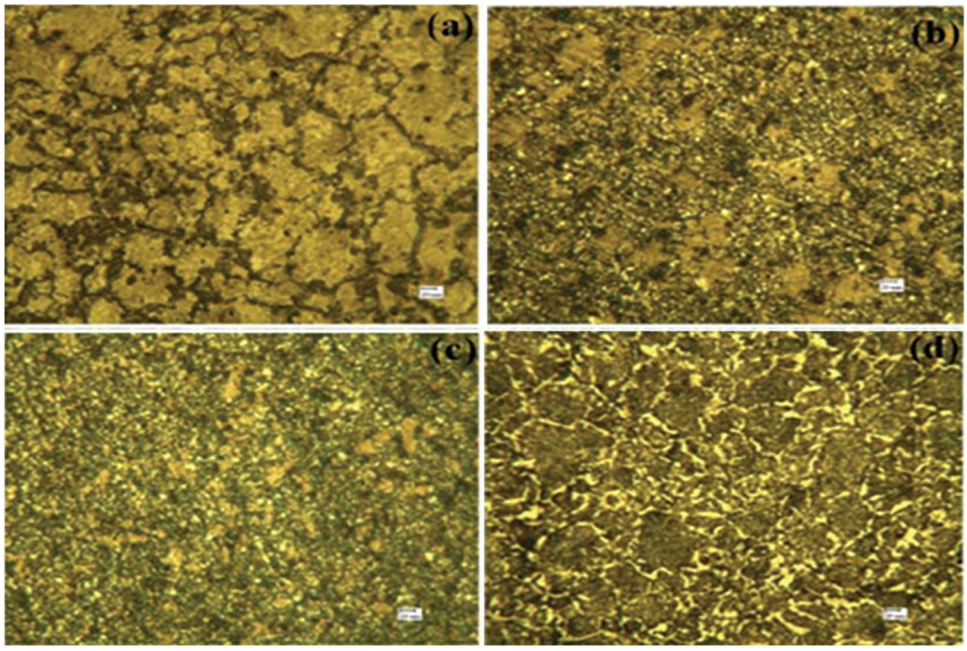

Figure 10: The microstructure of AISI 1045 steel specimens.

3.4.2. Optical microscopy of 1045 steel

At lower hardening temperatures, an incomplete martensite was formed, resulting in a decrease in surface hardness. Surface hardness increased consistently from 464 HV to 683 HV from 800 °C to 1200 °C. In a narrow temperature range of about 1100 °C, the number of martensitic structures grows, and at 1200 °C, the transformation is complete. The test produced a fully martensitic structure, as seen in the following image. Figure 10 is an optical micrograph of AISI 1045 steel that was heated to 1100 °C and then cooled in water. Figure 10 (a) & (b) shows an untempered specimen with an acicular shape due to the development of martensitic morphology. Figure 10 (c) & (d) shows decomposition to ferrite and carbide combinations at 300 °C, 500 °C, and 700 °C tempering temperatures, respectively.

4. INFLUENCE OF PROCESSING TEMPERATURES IN AISI 1045 STEEL

Experiments and processing are conducted at both low and high temperatures. The temperature has a major effect on the properties of AISI 1045 steel. Materials of high thickness and hardness may be made by raising the treatment temperature even higher [24–30]. This experiment, the low-temperature plasma nitro-carburizing on the surface of AISI 1045 steel. As the temperature rises, the surface may become harder and more resistant to wear. Hence, analyse the effects of processing temperature on AISI 1045 steel.

4.1. Experimental design and material selection

4.1.1. Selection of materials

Low hardness, wear resistance, and poor friction are characteristics of austenitic AISI steel. Nickel, manganese, and nitrogen are all present in AISI 1045 steel. Austenitic stainless steel is made by combining AISI 1045 steel with stabilisers such as nitrogen, copper, and cobalt. The major goal of nitrogen addition is to stabilise the austenite, which is formed in opposition to the development of ferrite at high temperatures and martensite at low temperatures.

4.1.2. AISI 204 Cu austenitic stainless steel

Alloy The austenitic stainless steel AISI 204 Cu is a combination of chromium and magnesium, and it also contains nitrogen and copper. The alloy is more malleable since copper was added to it. Copper increases corrosion and stress corrosion cracking resistance in several media. Adding nitrogen to the AISI 204 Cu alloy improves its mechanical qualities, particularly its temperature strength. Adding manganese to a material increases its tensile strength and hardness [31]. In the austenitic stainless steel rods according to AISI 204 and these stainless steel

Table 4: The chemical composition of AISI 204 Cu austenitic stainless steel.

COMPOSITION	C	Mn	Cr	Ni	Mo	Si	Cu	N	P	S	Fe
(%)	0.034	8.3	16.03	1.78	0.12	0.43	2.01	0.15	0.031	0.0022	Bal

materials outperform other stainless steels in terms of tensile strength and hardness. In corrosion-resistant settings, AISI 204 Cu stainless steel products excel. The chemical and elemental make ups of AISI 204 Cu austenitic stainless steel components are shown in table 4. Iron (Fe) is the primary element in AISI 204 Cu austenitic stainless steel. Chrome and manganese are two other elements that are found in AISI 204 Cu stainless steel in greater amounts.

4.1.3. Improving surface hardness and wear resistance of 1045 steel

This experimental work describes the methods used to increase the surface hardness and wear resistance of 1045 steel. The sample die used in these experiments has a 20 mm diameter and a 5 mm height. After cleaning and polishing, the sample specimens are placed into the pulsed plasma ion nitriding apparatus. After closing and pumping the vacuum chamber down to 6.65 Pa, further surface cleaning is performed at a temperature of roughly 300 °C for 40 minutes using a voltage of 350 V. Pulse times of 135 seconds are used for the plasma nitro-carburizing procedure.

4.1.4. Heat treatment by plasma nitro-carburizing

Nitrogen, hydrogen, and methane gas mixtures are discharged at temperatures between 300 and 460 °C for around 15 hours. These operations focus on temperature effects in order to describe the layered surface formed on austenitic AISI 1045 steel by plasma nitro-carburizing. After the treatments are complete, the sample is cooled to a normal temperature by being evacuated in a vacuum chamber. Etching is performed using special reagents consisting of 20% water, 30% HNO_3, and 50% HCl on the polished cross-sectional surface. After processing is complete, the microstructure and hardness are analysed process of plasma nitro-carburizing austenitic AISI 1045 steel. These treatments enhance the stainless steel wear resistance, surface hardness, and other properties. Plasma nitro-carburizing and metallographic analyses are performed on the samples in this experiment.

4.1.5. X-ray diffraction analysis (XRD)

XRD is a unique technique for establishing whether or not a substance is crystallised. Unknown crystalline materials, such as minerals, inorganic compounds, etc., may often be recognised via the use of these analytical techniques. The D/Max-200 X-ray diffractometer was used to examine the phase development across the plasma-treated surface. The microhardness is measured with a Vickers Hardness Tester (Mitutoyo), using a 50 gm indentation load for 15 s. Figure 11 shows the X-ray diffraction patterns obtained by processing the hardened layer at 300–460 °C for 15 hours at a pressure of about 5.32×10^2 Pa.

Figure 11 displays the findings of an XRD examination of nitro-carburized layers produced on AISI 1045 steel at different treatment temperatures. As treatment temperatures rise, the diffraction peaks at the treated surfaces move to smaller incidence angles. The addition of carbon and nitrogen atoms to a face-centered cubic structure causes the lattice to become distorted and grow in size, as seen above. It generates new phases that are nitrogen-enriched at the surface and carbon-enriched further in. It demonstrates that increased quantities of carbon and nitrogen atoms result from the regulated diffusion process under more extreme conditions [32–36]. In another section, when compared to the specimen tested at 400 °C, the diffraction peaks shift to an angle that is in a higher mode. By releasing nitrogen atoms, the formation of NCr_2 in the nitrogen-enriched layer reduces the lattice's deformation and growth. Increasing the treatment temperature all the way to 460 °C improves the phase quality.

Figure 12 depicts the resulting concentration patterns of carbon and nitrogen at a range of temperatures. There is abundant carbon underneath the enhanced nitrogen, as shown by the resultant dual layer structure. Heating to 400 °C increases the concentrations of carbon and nitrogen in the depth and surface of penetration.

Figure 12 displays carbon and nitrogen concentrations in nitro-carburized layers formed on AISI 1045 steel at various temperatures. This shows that at this temperature, the rate at which carbon and nitrogen atoms move into the steel is higher than the rate at which atoms return to the surface after the plasma. At higher temperatures, more carbon and nitrogen atoms move into the steel, carbon and nitrogen atoms will penetrate the substrate materials [37–39]. When it comes to diffusion, carbon in austenite moves around more quickly than nitrogen. As nitrogen becomes more soluble, its concentration near the surface goes up. This makes carbon

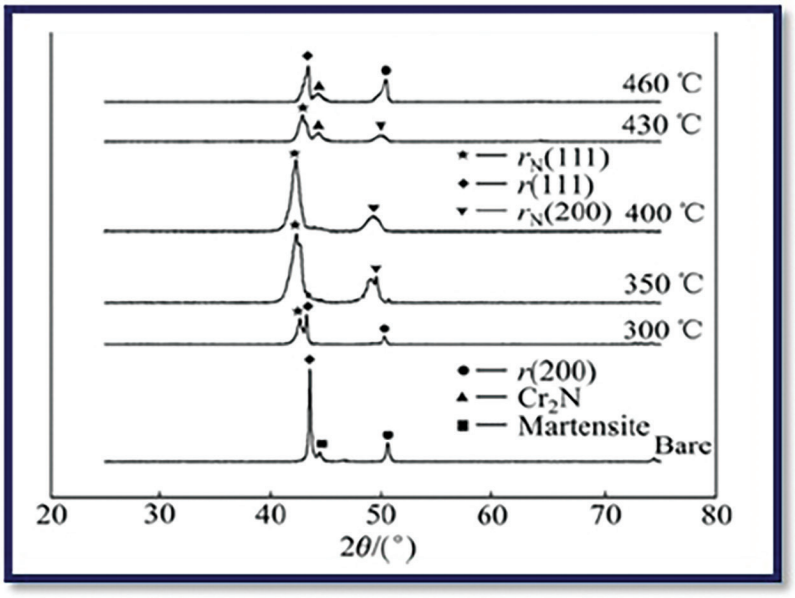

Figure 11: The XRD analysis of nitro-carburized layers of AISI 1045 steel.

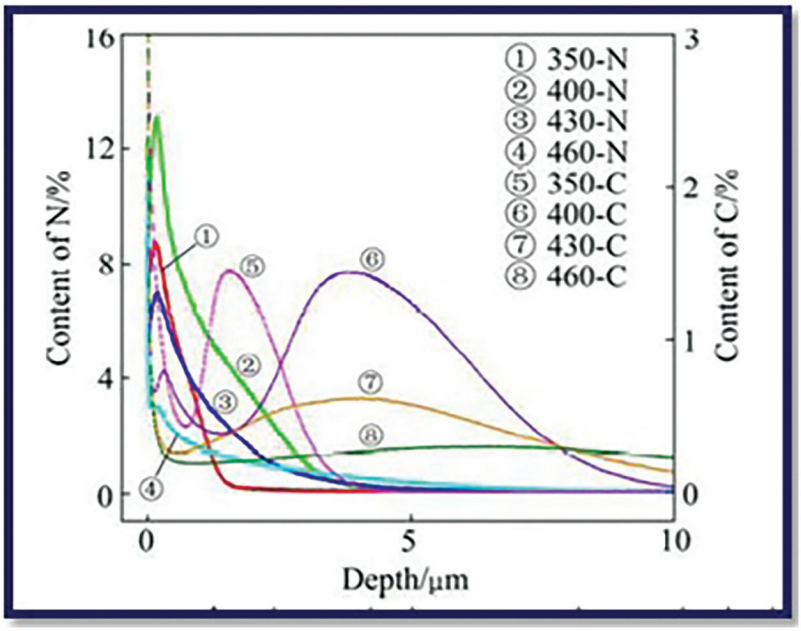

Figure 12: The contents of carbon and nitrogen on nitro-carburized layers.

atoms move deeper into the crystalline structure, where they can no longer contribute to the hardened layer. So, the plasma nitro-carburizing process is a combination of the low-temperature nitriding and carburizing processes.

4.1.6. Optical microscopy analysis

Using an optical microscope, the microstructure of nitro-carburized layers was examined. Figure 13 shows the morphology of AISI 1045 steel in cross-section, and the GDS measurements of carbon and nitrogen enrichment in the hardened layer. XRD analysis confirms the presence of NCr_2 precipitation within the nitrogen-enriched coating at temperatures above 430 °C. The hardened layer has decent corrosion resistance in comparison to the substrate material, as evidenced by its bright presence under an optical microscope and its insensitivity to the etchant (30 percent HNO_3 + 50 percent HCL + 20 percent H_2O, volume fraction).

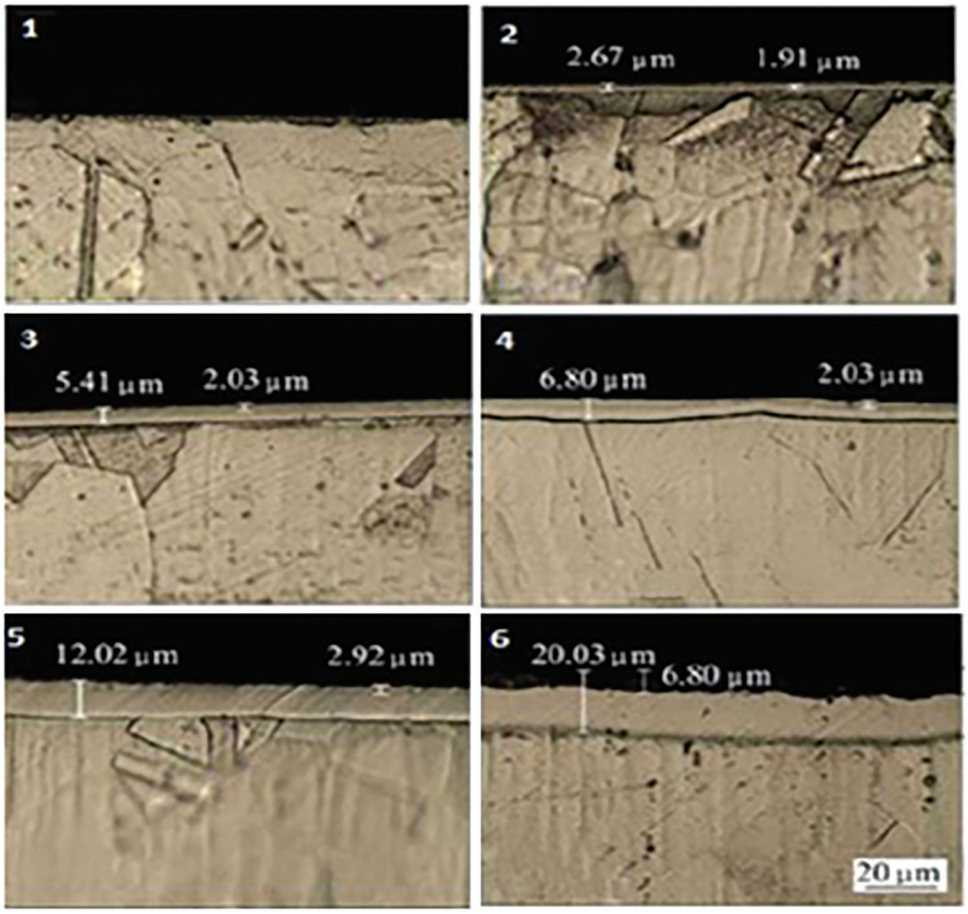

Figure 13: The cross-sectional view of nitro-carburized layers of specimen.

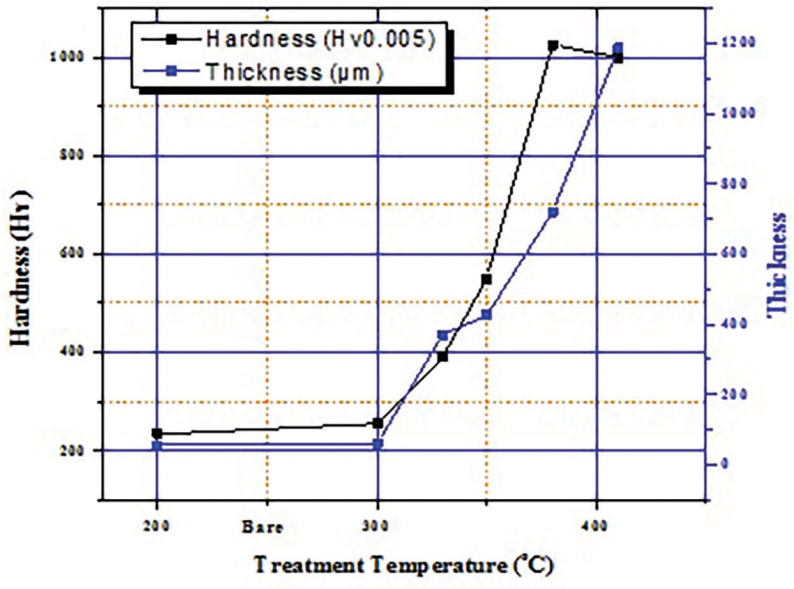

Figure 14: Thickness and surface hardness of nitro-carburized layers of the specimen.

The thickness and surface hardness of nitro-carburized layers generated on AISI 1045 steel at different processing temperatures are shown in Figure 14. Chromium nitride precipitation reduces corrosion resistance and the thickness of the hardened layer may be altered by varying the treatment temperature. During a 15-hour test, it was found that both the surface hardness and the thickness of the nitrocarburized layer depend on the temperature.

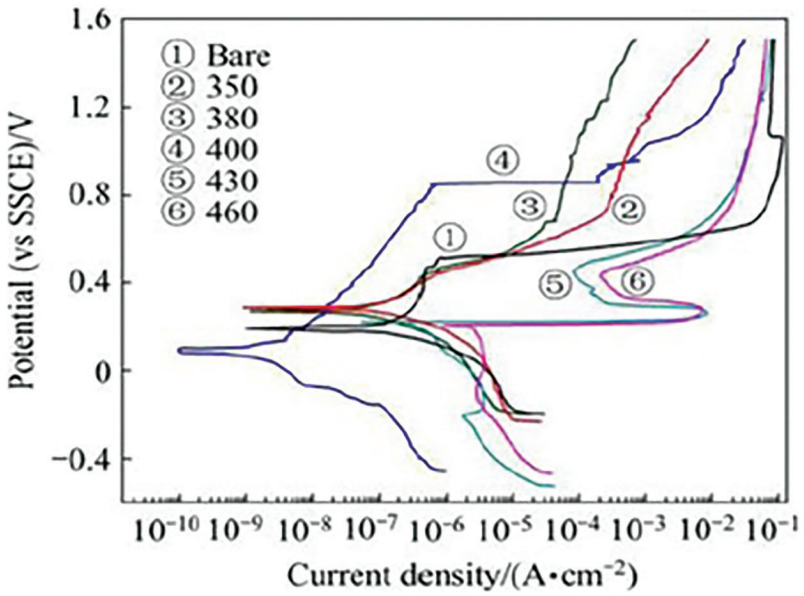

Figure 15: The polarization curves of nitro-carburized layers.

The influence of the substrate material may be mitigated by choosing an indentation load of 15 gm or less, which corresponds to the minimum thickness of the nitro-carburized layer. To a certain extent, the surface layer's stability increases in proportion to its thickness. When hydrogen and carbon are introduced into the interstices of FCC austenitic stainless steel, the resulting lattice distortion and growth is characteristic of the material [40, 41]. Because of the possibility of generating internal stress, surface hardness is increased, and dislocation motion is slowed. The sample's surface hardness was increased by a factor of four, from HV0.05 to HV1000, after treatment ($230HV_{0.05}$).

The temperature-dependent polarisation curvatures of the layers in a 3.5% sodium chloride solution are depicted in Figure 15. When the specimen is heated to 400 °C, the corrosion density is reduced in a proportional manner. The presence of a high concentration of nitrogen on the surface of the austenite increases corrosion resistance, and this is thought to be the result of an increase in pH caused by the formation of NH + (N+ 4H + 3e- NH+) in the acid pits, which in turn increases the passivation capacity and slows down the corrosion rate. The specimen passes the 400 °C test when Corrosion resistance is increased alongside a decrease in current density of about 300 mV and a pitting potential of about 300 mV. Finally, at 400 °C and a potential of around 1500 mV, there was no pitting seen on the surface. AISI 1045 steel materials have been tested in two phases, and the results show that an increase in temperature improves both their surface hardness and their resistance to corrosion. Boriding, hardening, and tempering AISI 1045 steel improves its microhardness properties but reduces its tensile properties. The conversion from AISI 1045 steel to AISI 204 Cu stainless steel enhanced the material's surface hardness, fatigue strength, wear resistance, and corrosion resistance. Plasma nitrocarburizing is a method that increases surface hardness. As the temperature rises, a carbon and nitrogen layer form on the surface, making it harder and more corrosion-resistant [42]. Because of its multilayer construction, AISI 1045 steel has increased strength.

5. CONCLUSION

This study analyses the effects of temperature on the surface hardness of AISI 1045 steel and provides a characterization of this material. Phase one of the experiments, the effects of processing temperature on the surface hardness of AISI 1045 steel through the use of boriding, hardening, and tempering. In the initial stage of testing, AISI 1045 steel materials are improved by induction boriding, material hardening, and tempering processes. At 1200 °C, a maximum hardness of 685 HV is achieved, with lower hardness values distinguished between 800 °C – 1100 °C. Because of the tempering procedure, martensite is structurally decomposed into a ferrite-carbide combination. The low temperature of 400 °C in the second phase of the experiments produces a sub-layer without precipitation and an austenite structure. Surface hardness and corrosion resistance were improved due to the formation of a dual layer structure consisting of a nitrogen-enriched layer above a carbon-enriched layer. When the treatment temperature is raised, the layer thickness increases to 20 m, and the surface hardness increases to 1000 $HV_{0.05}$. Since NCr_2, a nitrogen-enriched layer, forms at temperatures over 430 °C, corrosion resistance improves at higher

temperatures. When heated, AISI 1045 steel materials exhibit both increased corrosion resistance and surface hardness, with the latter reaching a maximum at 430 °C. AISI 1045 steel materials' surface hardness is found to increase with temperature during the hardening and tempering process, followed by water quenching.

6. REFERENCES

[1] MAJHI, K., BERTOLUZZI, L., KELLER, D.A., *et al*., "Co_3O_4 based all-oxide PV: a numerical simulation analyzed combinatorial material science study", *The Journal of Physical Chemistry C*, v. 120, n. 17, pp. 9053–9060, 2016. http://dx.doi.org/10.1021/acs.jpcc.6b01164

[2] FALCH, K.V., CASARI, D., DI MICHIEL, M. *et al.*, "In situ hard X-ray transmission microscopy for material science", *Journal of Materials Science*, v. 52, n. 6, pp. 3497–3507, 2016. https://doi.org/10.1007/s10853-016-0643-8

[3] FENG, H., CHEN, L., LIU, X., *et al*., "Constructal design for an iron and steel production process based on the objectives of steel yield and useful energy", *International Journal of Heat and Mass Transfer*, v. 111, pp. 1192–1205, 2017. http://dx.doi.org/10.1016/j.ijheatmasstransfer.2017.04.096

[4] LEVY, A., MIRIYEV, A., ELLIOTT, A., *et al*., "Additive manufacturing of complex-shaped graded TiC/steel composites", *Materials & Design*, v. 118, pp. 198–203, 2017. http://dx.doi.org/10.1016/j.matdes.2017.01.024

[5] ZHANG, Z., JING, H., XU, L., *et al*., "Influence of microstructure and elemental partitioning on pitting corrosion resistance of duplex stainless steel welding joints", *Applied Surface Science*, v. 394, pp. 297–314, 2017. http://dx.doi.org/10.1016/j.apsusc.2016.10.047

[6] GAO, K., QIN, X., ZHU, Z., *et al*., "Effect of surface curvature on tribological performance of AISI 1045 steel after multi-scan spot continual induction hardening process", *Tribology International*, v. 118, pp. 256–263, 2018. http://dx.doi.org/10.1016/j.triboint.2017.10.004

[7] ZHU, Y.P., GUO, C., ZHENG, Y., *et al*., "Surface and interface engineering of noble-metal-free electrocatalysts for efficient energy conversion processes", *Accounts of Chemical Research*, v. 50, n. 4, pp. 915–923, 2017. http://dx.doi.org/10.1021/acs.accounts.6b00635

[8] XI, X., XIA, Y., HU, Y., "The effects of magnetic treatment on the tribological behaviour of aisi 1045 steel under lubricated conditions", *Tribology Transactions*, v. 61, n. 4, pp. 1–12, 2018. https://doi.org/10.1080/10402004.2017.1390180

[9] JOMAA, W., SONGMENE, V., BOCHER, P., "An investigation of machining-induced residual stresses and microstructure of induction-hardened AISI 4340 steel", *Materials and Manufacturing Processes*, v. 31, n. 7, pp. 838–844, 2015. https://doi.org/10.1080/10426914.2015.1070431

[10] BARGLIK, J., SMALCERZ, A., SMAGOR, A., *et al*., "Experimental stand for investigation of induction hardening of steel elements", *Metalurgija*, v. 57, n. 4, pp. 341–344, 2018. https://hrcak.srce.hr/201760

[11] MEDINA-CLAVIJO, B., SAEZ-DE-BURUAGA, M., MOTZ, C., *et al*., "Microstructural aspects of the transition between two regimes in orthogonal cutting of AISI 1045 steel", *Journal of Materials Processing Technology*, v. 260, pp. 87–96, 2018. http://dx.doi.org/10.1016/j.jmatprotec.2018.05.016.

[12] FU, X., WANG, B., TANG, X., *et al*., "Study on induction heating of workpiece before gear rolling process with different coil structures", *Applied Thermal Engineering*, v. 114, pp. 1–9, 2017. http://dx.doi.org/10.1016/j.applthermaleng.2016.11.192

[13] MROZEK, K., CHEN, S.C., "Selective induction heating to eliminate the fudamental defects of thin-walled moldings used in electrical industry", *Journal of Applied Polymer Science*, v. 134, pp. 44992, 2017. http://dx.doi.org/10.1002/app.44992

[14] HAN, K.T., CHAU, K.T., ZHANG, Z., *et al*., "Flexible induction heating using magnetic resonant coupling", *IEEE Transactions on Industrial Electronics*,v. 64, n. 3, pp. 1982–1992, 2017. http://dx.doi.org/10.1109/TIE.2016.2620099

[15] HAN, W., CHAU, K., ZHANG, Z., *et al*., "Single-source multiple-coil homogeneous induction heating", *IEEE Transactions on Magnetics*, v. 53, pp. 111–116, 2017. http://dx.doi.org/10.1109/INTMAG.2017.8007681

[16] FISK, M., LINDGREN, L.-E., DATCHARY, W., *et al*., "Modelling of induction hardening in low alloy steels", *Finite Elements in Analysis and Design*, v. 144, pp. 61–75, 2018. http://dx.doi.org/10.1016/j.finel.2018.03.002

[17] FELDSHTEIN, E., JÓZWIK, J., LEGUTKO, S., *et al*., "The influence of the conditions of emulsion mist formation on the surface roughness of AISI 1045 steel after finish turning", *Advances in Science and Technology Research Journal*, v. 10, n. 30, pp. 144–149, 2016. http://dx.doi.org/10.12913/22998624/62773

[18] GNANA PRASANNA, N., RAJKUMAR., R., MICHAEL RAJ, F., "Non-destructive evaluation from deformed aluminum alloy 6063 and silicon carbides black and green reinforced aluminium alloy based composites", *Materials Express*, v. 12, pp. 1–11, 2022.

[19] KEDDAM, M., CHEGROUNE, R., KULKA, M. *et al.*, "Characterization, tribological and mechanical properties of plasma paste borided AISI 316 steel", *Transactions of the Indian Institute of Metals*, v. 71, pp. 79–90, 2017. https://doi.org/10.1007/s12666-017-1142-6

[20] XU, D.M., LI, G.Q., WAN, X.L., *et al*., "Deformation behavior of high yield strength–High ductility ultrafine-grained 316LN austenitic stainless steel", *Materials Science and Engineering A*, v. 688, pp. 407–415, 2017. http://dx.doi.org/10.1016/j.msea.2017.02.009

[21] SACKL, S., ZUBER, M., CLEMENS, H., *et al*., "Induction tempering vs conventional tempering of a heat-treatable steel", *Metallurgical and Materials Transactions. A, Physical Metallurgy and Materials Science*, v. 47, n. 7, pp. 3694–3702, 2016. http://dx.doi.org/10.1007/s11661-016-3534-3

[22] MARUDA, R.W, KROLCZYK, G.M., FELDSHTEIN, E., *et al*., "Tool wear characterizations in finish turning of AISI 1045 carbon steel for MQCL conditions", *Wear*, v. 372, pp. 54–67, 2017. https://doi.org/10.1016/j.wear.2016.12.006

[23] KRELLING, A.P., DA COSTA, C.E., MILAN, J.C.G., *et al*., "Micro-abrasive wear mechanisms of borided AISI 1020 steel", *Tribology International*, v. 111, pp. 234–242, 2017. http://dx.doi.org/10.1016/j.triboint.2017.03.017

[24] BARGLIK, J., SMALCERZ, A., "Influence of the magnetic permeability on modeling of induction surface hardening", in: https://doi.org/10.1108/COMPEL-05-2016-0240. *COMPEL:The International Journal for Computation and Mathematics in Electrical and Electronic Engineering*, v. 36, n. 2, pp. 555–564, 2017.

[25] JAFARIAN, M., RIZI, M.S., JAFARIAN, M., *et al*., "Effect of thermal tempering on microstructure and mechanical properties of Mg-AZ31/Al-6061 diffusion bonding", *Materials Science and Engineering A*, v. 666, pp. 372–379, 2016. http://dx.doi.org/10.1016/j.msea.2016.04.011

[26] IMRAN, M., KHAN, A.R.A., MEGERI, S., *et al*., "Study of hardness and tensile strength of Aluminium-7075 percentage varying reinforced with graphite and bagasse-ash composites", *Resource-Efficient Technologies*, v. 2, n. 2, pp. 81–88, 2016. http://dx.doi.org/10.1016/j.reffit.2016.06.007

[27] SHAHEDI ASL, M., AHMADI, Z., PARVIZI, S., *et al*., "Contribution of SiC particle size and spark plasma sintering conditions on grain growth and hardness of TiB_2 composites", *Ceramics International*, v. 43, n. 16, pp. 13924–13931, 2017. http://dx.doi.org/10.1016/j.ceramint.2017.07.121

[28] POPESCU, A., DELVAL, C., LEPAROUX, M., *et al*., "Control of porosity and spatter in laser welding of thick AlMg5 parts using high-speed imaging and optical microscopy", *Metals*, v. 7, n. 11, pp. 452, 2017. http://dx.doi.org/10.3390/met7110452

[29] ALSALLA, H., HAO, L., SMITH, C., *et al*., "Fracture toughness and tensile strength of 316L stainless steel cellular lattice structures manufactured using the selective laser melting technique", *Materials Science and Engineering A*, v. 669, pp. 1–6, 2016. http://dx.doi.org/10.1016/j.msea.2016.05.075

[30] WANG, X., YAN, M., LIU, R., *et al*., "Effect of rare earth addition on microstructure and corrosion behavior of plasma nitrocarburized M50NiL steel", *Journal of Rare Earths*, v. 34, n. 11, pp. 1148–1155, 2016. http://dx.doi.org/10.1016/S1002-0721(16)60147-3

[31] GOVINDAN, K., MADAN SHANKAR, K., KANNAN, D., "Sustainable material selection for construction industry–A hybrid multi criteria decision making approach", *Renewable & Sustainable Energy Reviews*, v. 55, pp. 1274–1288, 2016. http://dx.doi.org/10.1016/j.rser.2015.07.100

[32] DE LA FUENTE, D., ALCÁNTARA, J., CHICO, B., *et al*., "Characterisation of rust surfaces formed on mild steel exposed to marine atmospheres using XRD and SEM/Micro-Raman techniques", *Corrosion Science*, v. 110, pp. 253–264, 2016. http://dx.doi.org/10.1016/j.corsci.2016.04.034

[33] BAUMERS, M., DICKENS, P., TUCK, C., *et al*., "The cost of additive manufacturing: machine productivity, economies of scale and technology-push", *Technological Forecasting and Social Change*, v. 102, pp. 193–201, 2016. http://dx.doi.org/10.1016/j.techfore.2015.02.015

[34] GOPAL, K.V.N., "Product design for advanced composite materials in aerospace engineering", In: RANA, S., FANGUEIRO, R. (eds), *Advanced composite materials for aerospace engineering*, USA: Elsevier, 2016. pp. 413–428.

[35] ATLATI, S., MOUFKI, A., NOUARI, M., *et al*., "Interaction between the local tribological conditions at the tool–chip interface and the thermomechanical process in the primary shear zone when dry machining the aluminum alloy AA2024–T351", *Tribology International*, v. 105, pp. 326–333, 2017. https://doi.org/10.1016/j.triboint.2016.10.006

[36] CHEN, P.-J., ZHU, C.-Y., LI, G.-Q., *et al*., "Effect of sulphur concentration on precipitation behaviors of MnS-containing inclusions in GCr15 bearing steels after LF refining", *ISIJ International*, v. 57, n. 6, pp. 1019–1028, 2017. https://doi.org/10.2355/isijinternational.ISIJINT-2017-007

[37] XUE, Y.-X., YOU, J.-X., LAI, X.-D., *et al*., "An interval-valued intuitionistic fuzzy MABAC approach for material selection with incomplete weight information", *Applied Soft Computing*, v. 38, pp. 703–713, 2016. http://dx.doi.org/10.1016/j.asoc.2015.10.010

[38] HAUBNER, R., LESSIAK, M., PITONAK, R., *et al*. "Evolution of conventional hard coatings for its use on cutting tools", International Journal of Refractory Metals and Hard Materials, vol. 62, pp. 210–218, 2017. https://doi.org/10.1016/j.ijrmhm.2016.05.009

[39] ADHIKARI, P., MIRSHAMS, R., "Study of knowledge-based system (KBS) and decision making methodologies in materials selection for lightweight aircraft metallic structures", *Journal of Applied Science & Engineering Technology*, v. 5, pp. 1–19, 2017.

[40] RAJKUMAR, R., GNANA PRASANNA, N., MICHAEL RAJ, F., "Influence of processing parameters on AA 6063/SiC (Black & Green) composites in wire EDM", *Tierärztliche Praxis*, v. 53, n. 2, pp. 1966–1990, 2019.

[41] CHEN, C., ZENG, X., WANG, Q., *et al*., "Statistical modelling and optimization of microhardness transition through depth of laser surface hardened AISI 1045 carbon steel", *Optics & Laser Technology*, v. 124, pp. 105976, 2020. https://doi.org/10.1016/j.optlastec.2019.105976

[42] MENG, Y., DENG, J., ZHANG, Y., *et al*., "Tribological properties of textured surfaces fabricated on AISI 1045 steels by ultrasonic surface rolling under dry reciprocating sliding", *Wear*, n. 203488, pp. 460–461, 2020. https://doi.org/10.1016/j.wear.2020.203488